Optical Properties of Metal Tips for Tip-Enhanced Spectroscopies†

Maxim Sukharev*,‡ and Tamar Seideman*,§

Chemistry, Physics, and Applied Mathematics, Arizona State University at the Polytechnic Campus, 6073 S. Backus Mall, Mesa, Arizona 85212, and Department of Chemistry, Northwestern University, 2145 Sheridan Road, Evanston, Illinois 60208

Received: January 29, 2009; Revised Manuscript Received: March 4, 2009

We develop a full 3D approach to simulate the optical properties of sharp metal tips that could be quantitatively compared with experiments and provide accurate predictions. Similar to metallic wires, elongated metal tips support a series of extended mode resonances whose properties are largely determined by the tip geometry and are essentially independent of the tip material. For sufficiently long tips, these resonances are energetically well separated from a broader, high-energy feature, whose position and line shape are independent of the tip length but vary strongly with the tip material. The latter is a localized plasmon mode characterized by the hemisphere terminating the tip.

1. Introduction

The interaction of light with sharp metallic tips is of both fundamental and pedagogical interest, and has been the topic of rapidly increasing scientific inquiry for its relevance to a variety of tip-enhanced spectroscopies. Similar to metal surfaces and metal nanoparticles, sharp noble metal tips give rise to enhancement and spatial localization of incident light at plasmon resonance frequencies, where the light frequency matches the frequency of collective excitation of the free electrons confined in the particle. The case of a noble metal tip, however, has unique features that distinguish it from the extensively studied surface and nanoparticle cases. From the theoretical perspective, the tip is neither finite nor periodic—it is an open system and hence exhibits specific effects and requires specific methods. It also provides a very simple model of a classic resonator. From the practical perspective, metal tips play a role in a variety of emerging applications. These include tip-enhanced Raman spectroscopy,[1−4] currently reaching the long-sought limit of single molecule detection;[5] chemical analysis with ultratrace sensitivity based on selective removal of sample material by an atomic force microscope (AFM) tip;[2] near-field optical imaging, enabled by scanning near-field optical microscopy (SNOM);[6] and ultrafast scanning tunneling microscopy—the combination of a tip with ultrashort laser pulses to combine nanoscale spatial resolution with femtosecond temporal resolution.[7]

Closely related physics gives rise to optical emission from tips.[8−10] Here, the proximity of the tip and the surface in the scanning tunneling microscope (STM) environment gives rise to tip-induced plasmons, excited by inelastic electron tunneling. Optical emission from these localized electromagnetic modes provides a probe of the underlying electromagnetic interactions. Other interesting questions involved in the interaction of light with sharp metal tips, including spin-polarized tunneling, light-induced nanomodifications, and thermal effects and nonlinear effects, are reviewed in ref. 11.

From the numerical perspective, modeling the electromagnetic response of a metal tip is a challenge.[12−15] Reference 15 performed an extensive study of the optical properties of a 58 nm long silver tip of different tip radii in the vicinity of a glass substrate, using the Drude model to describe the dielectric constat. It noted the appearance of an artificial feature at $\lambda =$ 505 nm, which is large and broad, and hence dominating over the physical localized mode at $\lambda = 541$ nm. Studies of the tip length effect in the 74−118 nm range, carried out to evaluate the validity of the model, found two series of broad features that are red-shifted and become increasingly dominant as the tip length grows. It was concluded that the system could be considered to approximate the extended tip in the absence of the artificial extended modes corrupting the spectra. For a true extended tip we may expect to recover a response from just the localized mode. Reference 15 proposed further that "The failure of boundary conditions where the tip meets the boundary is likely to arise from deficiencies in the use of a buffer layer with frequency-independent dielectric response".

As the experimental interest in tip-enhanced spectroscopies and tip-enabled control continues to grow, we present, in the present work, a numerical study of the optical properties of a metallic tip that addresses the challenges that were pointed out, but not yet met in the previous literature. Since the high-energy localized plasmon mode was studied in some detail in refs 12−15, we focus here primarily on the extended modes of the tip, which contain the physics of the open system and are essentially independent of the tip material. Since, however, the present study allows us to fully disentangle the localized plasmon mode from the extended modes, and since the former is typically the resonance of experimental interest, we provide a brief discussion of those of its features that have not been explored in the previous literature. The reader is referred to ref 14 for an extensive discussion of the effect of the tip−surface separation and to ref 15 for studies of the tip radius and light polarization dependencies of the localized plasmon resonance.

The next section outline our numerical method and section 3 presents and discusses the results. The final section concludes with a review of relevant literature and a discussion of avenues for future research.

† Part of the "Robert Benny Gerber Festschrift".

* To whom correspondence should be addressed. E-mail: maxim.sukharev@asu.edu (M.S.); t-seideman@northwestern.edu (T.S.).

‡ Arizona State University at the Polytechnic Campus.

§ Northwestern University.

10.1021/jp900877m CCC: $40.75
Published on Web 04/08/2009

2. Numerical Approach

The optical response of the metal tip is simulated using a finite-difference time-domain (FDTD) approach in three dimensions.[16] The simulation setup is shown in the inset of Figure 1, where an elongated conical metal tip of length L is placed at the center of the grid with its symmetry axis taken to define the Z-axis. Here R denotes the radius of the curvature at the end of the tip, and the red star marked by D under the tip apex indicates the spatial position of a near-field detector. In the simulations below, the detector is placed $D = 15$ nm below the tip apex. Perfectly matched layers (PML) absorbing boundaries are implemented in order to account for the open system boundary conditions.[17] The overall size of the FDTD cube is varied with the tip length, while the spatial step sizes are fixed at $\delta x = \delta y = \delta z = 1.5$ nm, which guarantees numerical convergence of the results with respect to the grid density. The temporal step is fixed at $\delta t = \delta x/(2c)$, where c is the speed of light in vacuum. Simulations are performed in parallel with the parallelization technique developed in ref. 18. All simulations utilize the Abe supercomputer at the National Center for Supercomputer Applications and the Saguaro cluster at Fulton School of Engineering and High Performance Supercomputer Center at Arizona State University.

To account for the material dispersion, we implement the auxiliary differential equation method[19] and both the standard Drude model and the more general Lorentz−Drude model.[20] Within the latter model, the dielectric permittivity is expressed as

$$\varepsilon(\omega) = \varepsilon_D(\omega) + \varepsilon_L(\omega) \quad (1)$$

where ε_D is a dielectric constant within the Drude approximation,

$$\varepsilon_D(\omega) = \varepsilon_\infty - \frac{{\omega_p}^2}{\omega^2 + i\Gamma_0\omega} \quad (2)$$

and ε_L is given as a sum of Lorentz damped oscillators,

$$\varepsilon_L(\omega) = \sum_n \frac{f_n {\omega_p}^2}{({\omega_n}^2 - {\omega_p}^2) + i\omega\Gamma_n} \quad (3)$$

In eq 2 ε_∞ is a dimensionless constant physically corresponding to the infinite-frequency limit of the dielectric function, ω_p is the bulk plasma frequency, and Γ_0 is a damping constant. In eq 3, each of the poles is specified by an oscillator strength, f_n, an oscillator frequency, ω_n, and a lifetime, $1/\Gamma_n$. The simulations presented in the next section used 5 poles, $n = 1,..., 5$, with the constants corresponding to the different materials studied. All parameter have been determined empirically in the previous literature.[21] Whereas the Lorentz−Drude model is more accurate than the Drude approximation, the latter model is less memory intensive, with a resulting shorter execution time. The Drude model is also the one used in previous studies[12−15] and is hence convenient for comparison with the previous literature. We therefore begin by comparing the results of the Drude and the Lorentz−Drude models for a silver tip; see Figure 1. The

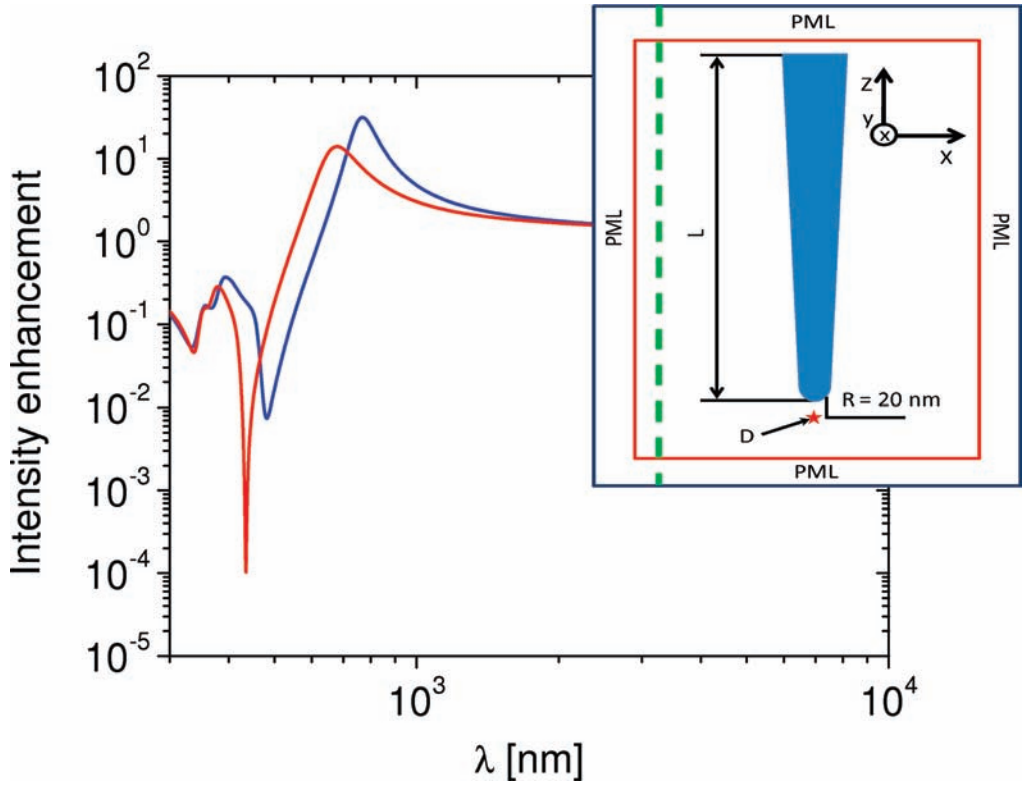

Figure 1. Inset shows schematically the simulations setup. A conical tip of length L is terminated by a hemisphere of radius R. The tip is aligned along the Z-axis and is exposed to an external, z-polarized plane wave pulse, generated along the vertical line shown on the left as a dashed green line. The intensity enhancement is determined at a detection point D, displaced from the tip apex by 15 nm. The main panel shows the intensity enhancement due to a silver tip of 100 nm length and a tip apex of 20 nm radius as a function of the incident wavelength. The blue curve shows data obtained using the general Lorentz−Drude model (see eq 1), and the red curve shows simulations utilizing the Drude model (see eq 2).

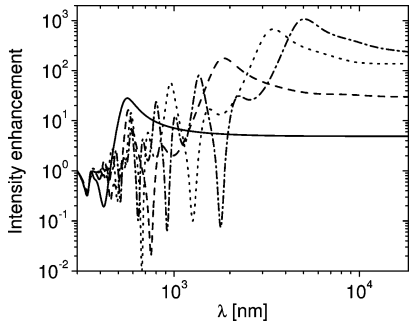

Figure 2. Intensity enhancement computed using the Drude model (see eq 2) as a function of the incident wavelength for a silver tip of different lengths: $L = 100$ nm (solid curve), $L = 500$ nm (dashed curve), $L = 1$ μm (dotted curve), $L = 1.5$ μm (dash-dotted curve). The radius of the apex curvature is fixed at $R = 20$ nm.

subsequent results are based on both models, restricting the application of the Drude model to questions to which its validity has been confirmed.

Several observables are computed in an effort to understand the plasmonic physics associated with tip enhancement and to develop a numerical approach that can be quantitatively compared with experiments. To simulate the spectral properties of the system, we apply an ultrashort, linearly polarized pulse along the vertical line shown in dashed green in the inset of Figure 1. The incident pulse duration is chosen such that the bandwidth will span the range of wavelengths of interest. After exciting the system, the incident pulse is absorbed by the PML boundaries and the electromagnetic eigenmodes of the tip are detected at the detection point D. The time-dependent fields are then Fourier transformed to yield the optical spectrum. We propagate the Maxwell equations for 500 fs to achieve the desired frequency resolution. Steady-state intensity distributions at fixed incident wavelengths are calculated using a phasor-function approach,[16] which provides the eigenstates within a single FDTD run.

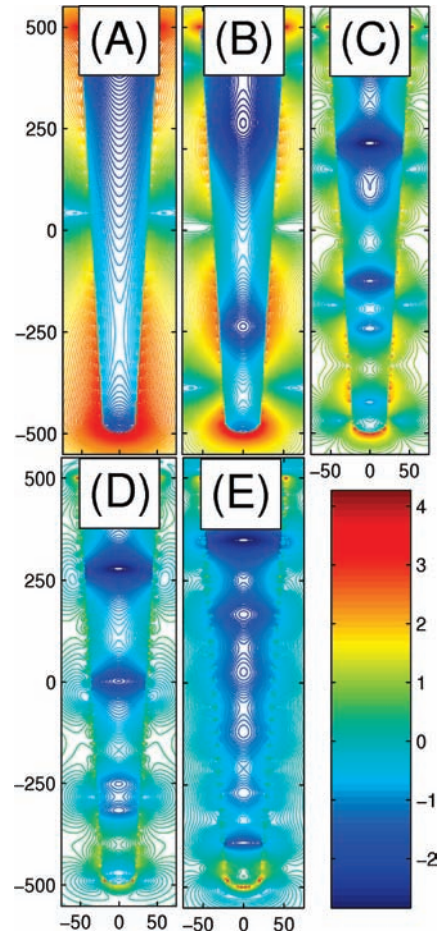

Figure 3. Intensity distributions in logarithmic scale for a 1 μm long silver tip at the energies of the resonances in Figure 2. See the text for a discussion and interpretation of the nodal structure. (A) The low-energy eigenstate at $\lambda = 5024$ nm, (B) $\lambda = 2221$ nm, (C) $\lambda = 1015$ nm, (D) $\lambda = 482$ nm. (E) The surface localized plasmon resonance at 363 nm. The radius of the apex curvature is fixed at $R = 20$ nm.

3. Results and Discussion

We open this section by testing the fidelity of the Drude model of eq 2 through direct comparison of its results with those of the more accurate Lorentz−Drude model (eq 1). Figure 1 illustrates the intensity enhancement for a silver tip at the detection point, denoted D in the inset, as a function of the incident wavelength, λ. Although the data obtained within the Drude model is noticeably blue-shifted with respect to that determined within the Lorentz−Drude approach, it nicely captures the main physical features of the system. Comparison of the two models for gold nanostructures (not shown), however, shows considerably less reliable performance.

Proceeding to explore the optical response of sharp metal tips, we first vary the tip length, L, and calculate the intensity enhancement below the tip apex for a fixed radius of curvature, $R = 20$ nm. Figure 2 illustrates the data obtained for four values of the tip length ranging from 100 nm to 1.5 μm. As L is increased, one observes more and more resonances, corresponding to the excitation of multipolar EM modes of the tip. Another evident feature is a red shift of the lowest energy resonance and a decrease of the energy spacings between each resonance and the one energetically above it with increase of the tip length.

Figure 3 illustrates the intensity enhancement distribution of the near field associated with different resonances for a tip length of 1 μm. The lowest energy resonance corresponds to a nodeless field distribution and is hence referred to below as the ground eigenstate. Owing to its nodeless structure, this resonance is the largest and broadest peak in all spectra, providing the greatest intensity enhancement. The higher energy peaks correspond each to an eigenstate with one additional node as compared to the resonance below it, and thus become more structured and lower in enhancement as the peak energy grows. Panel E of Figure 3 shows the high-energy resonance at $\lambda = 370$ nm, the physics of which is discussed below. For short tips the high-energy resonances overlap with the ground-state resonance and cannot be resolved, while longer tips support more states with properly isolated resonances. Finally, we note that the incident pulse polarization significantly affects the intensity enhancement,[15] resulting in negligibly small enhancements for Y-polarized incident fields. Simulations for gold and copper tips lead to similar results to the data obtained for silver. All features are expected from simple considerations of resonator-like systems. In particular, the enhancement for light polarized perpendicular to the tip axis (which excites a mode transverse to the tip axis) corresponds to a resonator of length $R/L \sim 0.2-0.013$ of that corresponding to the longitudinal mode, and hence provides negligible enhancement as compared to light polarized along the tip axis. A similar series of resonances has been experimentally found for silver[22] and gold[23] nanorods.

By gradual variation of the tip length, L, one obtains the resonant wavelength dependence of the energy-resolved EM eigenstates on L. Figure 4 shows data extracted from the optical

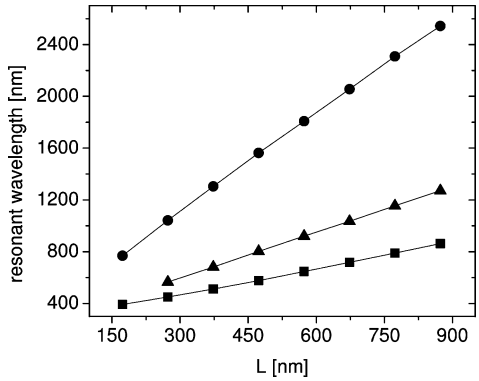

Figure 4. Resonance wavelength dependence on the tip length, L, for the lowest energy three EM eigenmodes of a silver tip with a fixed apex curvature of 20 nm. The data for the ground state is shown as circles, for the first excited EM eigenstate as triangles, and for the second excited EM state as squares. The simulations are based on the generalized Lorentz−Drude model (see eq 1 for details) with five poles.

spectra of silver tips of eight lengths ranging from 100 to 900 nm. The simulations are based on the generalized Lorentz−Drude model of eq 1. Two features are noted: first, the resonance wavelength is a linear function of the tip length with a positive slope, resulting in a red shift with increasing tip length. Second, with increase of the multipolar order, the slope decreases. This behavior is in the perfect agreement with experimental findings for silver nanorods.[22]

The most important characteristic of the calculated spectra is that all simulated tips, irrespective of their lengths, exhibit almost identical optical responses at high energies, below $\lambda =$ 370 nm. At frequencies well above the frequency of the longitudinal, extended tip states that result from collective oscillations along the tip axis, we observe the eigenmode of the hemisphere that terminates the tip. It is nicely illustrated by Figure 3E, where the EM field is mostly localized near the tip appex. This feature is essentially identical for z- and y-polarized light and is similar in peak position and spectral shape to the single resonance feature of a sphere of radius R. The transition from a series of discrete states to the continuum-like, single resonance of a classic sphere with increasing energy is thus a unique feature of tips and is governed by the optical features of the tip apex.

This result is quantified in Figure 5, where we show an expanded view of the high-energy edge of the eigenstate spectrum. Figure 5A illustrates the convergence of the results of different length tips to an identical feature in the short wavelength edge. Figure 5B shows the intensity enhancements associated with silver tips with $R = 20$ nm and $R = 40$ nm along with enhancements obtained for single silver spheres of the same radii. The correspondence between a sphere spectrum and a response of the tip with same radius illustrates that the high-energy ($\lambda \approx 350-370$ nm) EM state indeed derives from a localized surface plasmon resonance of the tip apex. The resonant wavelength, however, is perturbed with respect to the case of an ideal sphere, and the intensity enhancement line shape is modified. Increase of the sphere radius leads to a red shift, as expected from the general Mie theory.[24] The same red shift is observed also with increasing radius of the tip apex.

The appearance of a series of narrow resonances that correspond to the discrete resonator eigenmodes is a general feature of elongated plasmonic systems. These resonances are primarily determined by the tip geometry (see Figure 2) and are insensitive to the nature of the material. The latter feature

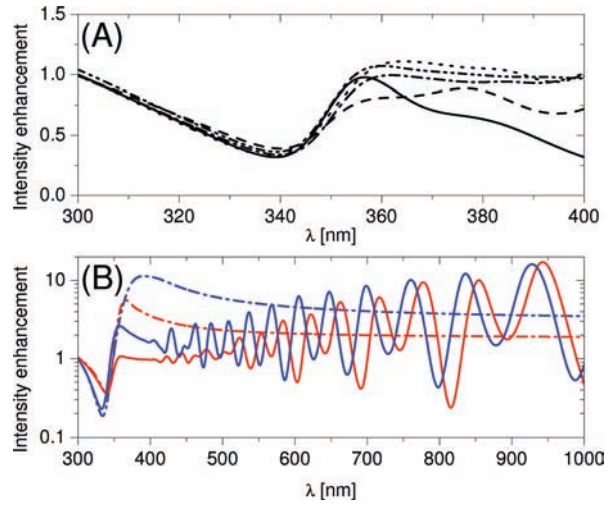

Figure 5. (A) High-energy part of the intensity enhancement spectrum as a function of the incident wavelength and the tip length L. $L = 100$ nm (solid curve), $L = 500$ nm (dashed curve), $L = 1$ μm (dotted curve), $L = 1.5$ μm (dash-dotted curve), $L = 3.6$ μm (dash-dot-dotted curve). The apex radius of the tip is $R = 20$ nm. (B) Intensity enhancement as a function of the incident wavelength for a silver tip (solid curves) and a single sphere (dot-dashed curves) with two radii: $R = 20$ nm (red curves) $R = 40$ nm (blue curves). The tip length is fixed at $L = 3.6$ μm.

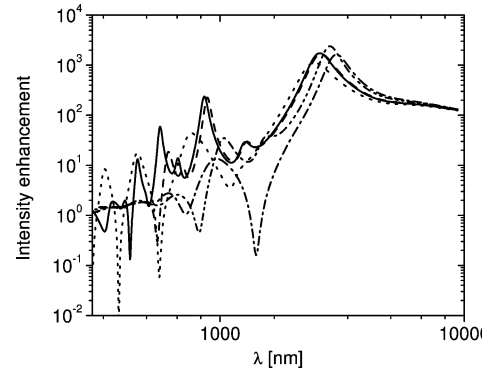

Figure 6. Intensity enhancement for an 800 nm long tip of different metals: Ag (solid curve), Au (dashed curve), Al (dotted curve), Pt (dash-dotted curve), and W (dash-dot-dotted curve). Simulations are performed utilizing the Lorentz−Drude model with $n = 5$ in eq 3. The radius of the apex curvature is fixed at $R = 20$ nm.

is illustrated in Figure 6, which provides the spectra of 800 nm long tips of five different metals: Ag, Au, Al, Pt, and W. The parameters of the dielectric functions used to determine the response of these materials are collected in Table 2 of ref 21a. It is evident that the line positions are independent of the dielectric function. By contrast, the plasmonic feature appearing at the high-energy edge is independent of the tip length (provided that it is sufficient to avoid overlap of the extended, geometric features with the plasmonic peak), but strongly dependent on the tip material; see Figure 6. Comparison of Figure 2 with Figure 6 thus associates the two parts of the spectrum with the different physical information contained in the low-energy extended modes and the high-energy localized plasmon mode.

We conclude this section by briefly comparing the intensity enhancement of an isolated tip with that resulting from a tip−surface system. Figure 7 illustrates the results of our simulations for a gold tip and a gold surface at different tip−surface distances. The intensity enhancement distributions are extracted from 3D FDTD data at three cuts through the 3D

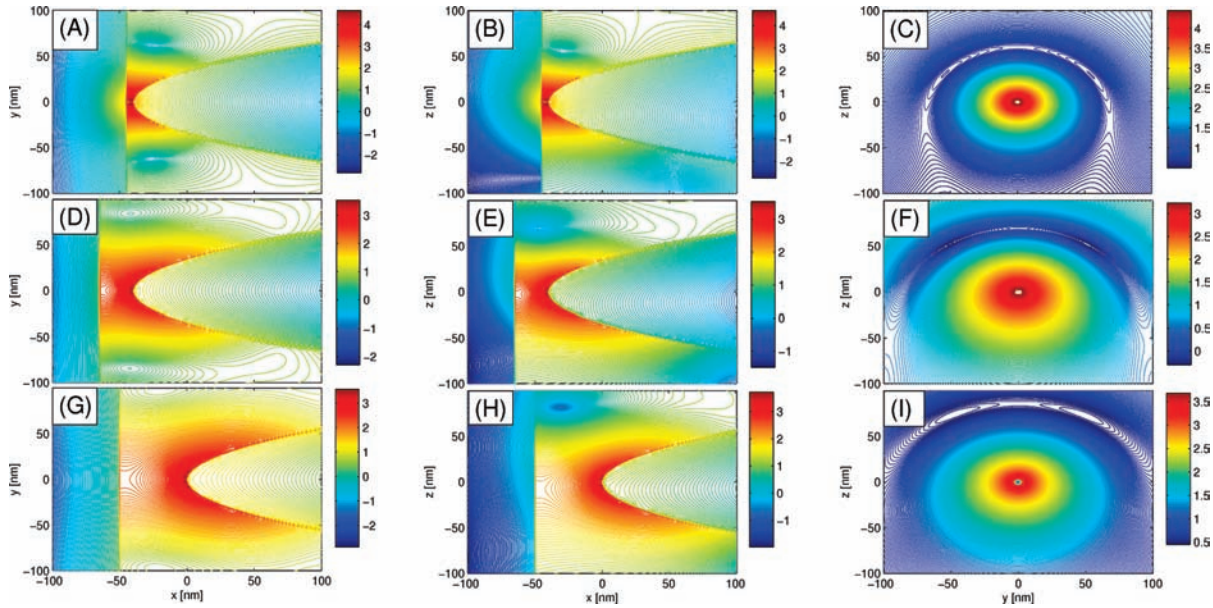

Figure 7. Two-dimensional cuts of the intensity enhancement (in logarithmic scale) for a gold tip placed near a gold surface at $\lambda = 450$ nm, corresponding to the localized surface plasmon resonance of the tip apex. The upper row (A, B, and C) shows data for a tip−surface distance of 10 nm, the middle row (D, E, and F) for 25 nm, and the bottom row (G, H, and I) for 50 nm. The system is excited with a linearly polarized laser pulse propagating along the negative *Z*-axis and polarized along *X*. The radius of the apex curvature is fixed at $R = 20$ nm.

space. The left column corresponds to $z = 0$, the middle column to $y = 0$, and the right column corresponds to the $x = 0$ plane. The origin of the coordinate system is just below the tip apex, hence the $z = 0$ and $y = 0$ planes symmetrically bisect the tip and the $x = 0$ plane is tangent to the terminating sphere. The intensity enhancement is sharply peaked below the tip apex, where the EM energy is focused due to both the localized plasmon enhancement by the tip apex and the propagating surface modes. The presence of a conducting surface in the vicinity of the tip significantly improves the EM field localization and hence increases the intensity enhancement. The smaller the tip-to-surface distance, the greater the enhancement. We note that the minimum tip-to-surface distance that can be reliably simulated within our classical framework is ca. 5 nm. At smaller distances, quantum effects need to be considered.[24] We also note that the peak enhancement is removed from the surface in all but the smallest tip−surface distances considered; hence, tip-enhanced spectroscopy of surface-adsorbed molecules requires rather close approach of the tip to the substrate.

An extensive discussion of the effect of the tip−surface distance on the plasmon mode is provided in ref 15 and is thus excluded from the present study.

4. Conclusion

Our goal in the research discussed in the previous sections has been to develop a realistic, full 3D approach to simulate the optical properties of a sharp metal tip that could be quantitatively compared with experiments and provide accurate predictions. We applied the model to understand and quantify the extended modes of the tip, corresponding to oscillations along the symmetry axis of the tip. The existence of such states has been discussed in an earlier numerical study,[15] but the resonance features could not be resolved with the tip lengths permitted by earlier numerical methods.

We found that the appearance of a long series of extended mode resonances is a general feature of elongated metal tips. Their properties are largely determined by the tip geometry and are essentially independent of the tip material. For sufficiently long tips, these resonances are energetically well separated from a broader, high-energy feature, whose position and line shape are independent of the tip length but vary strongly with the tip material. The latter is a localized plasmon mode, a feature of the hemisphere terminating the tip.

The recent theoretical and experimental literature suggests a variety of metallic nanoconstructs that are capable of improving the enhancement factor of conventional tips and could serve as efficient SERS media. Reference 4 proposes the gap between a pair of spheres in close vicinity as a potential SERS medium. Reference 25 illustrates that yet larger enhancements can be attained in gold nanoparticle−nanowire systems. Similarly large enhancements have been observed for periodic arrays. The extreme sensitivity of the enhancement factor to the fine geometric details of the nanoconstruct (including the radius of the hemisphere that terminates the tip, the cone half angle, the width, and length of the tip coating in the case of partially coated tips) has been likewise illustrated. This suggests the potential of a general numerical design tool that will yield an optimal tip structure subject to a set of experimental constraints and a desired target. Recently, we developed such a design algorithm for a general nanoplasmonic construct by combining the FDTD method with a genetic algorithm approach. The method was applied to the design of several plasmonic nanodevices with desired functionalities, including a metal nanolense, and a nanoscale light source with predetermined polarization. One of our goals in future research in this area will be to design metallic tips and tip−nanoparticle systems with advantageous properties and apply them to assist the design of spectroscopic and control experiments in molecular nanoplasmonics.

Acknowledgment. This work is dedicated to Prof. R. Benny Gerber, a friend, an educator, and an inspiring colleague, on the occasion of is 60th birthday. We thank the W. M. Keck Foundation and the NCLT program of the National Science Foundation (ESI-0426328) at the Materials Research Institute of Northwestern University for support. The numerical work discussed in this article used the resources of the National Center for Supercomputer Applications under grant No. TG-

MCA06N016. We also thank Fulton School of Engineering and High Performance Supercomputer Center at Arizona State University for supercomputing time at the Saguaro cluster that allowed us to perform long execution time simulations.

References and Notes

(1) Stöckle, R. M.; Suh, Y. D.; Deckert, V.; Zeno, R. *Chem. Phys. Lett.* **2000**, *318*, 131.
(2) Anderson, M. S. *Appl. Phys. Lett.* **2000**, *76*, 3130.
(3) Neacsu, C. C.; Dreyer, J.; Behr, N.; Raschke, M. B. *Phys. Rev. B* **2006**, *73*, 193406.
(4) Kodama, T.; Umezawa, T.; Watanabe, S.; Ohtani, H. *J. Microsc.* **2008**, *229*, 240.
(5) Greenleaf, W. J.; Woodside, M. T.; Block, S. M. *Annu. Rev. Biophys. Biomol. Struct.* **2007**, *36*, 171.
(6) Wiederrecht, G. P. *Eur. Phys. J. Appl. Phys.* **2004**, *28*, 3.
(7) Steeves, G. M.; Elezzabi, A. Y.; Freeman, M. R. *Appl. Phys. Lett.* **1998**, *72*, 504.
(8) Berndt, R.; Gimzewski, J. K.; Johansson, P. *Phys. Rev. Lett.* **1993**, *71*, 3493.
(9) Johansson, P. *Phys. Rev. B* **1998**, *58*, 10823.
(10) Nilius, N.; Ernst, N.; Freund, H.-J. *Phys. Rev. Lett.* **2000**, *84*, 3994.
(11) Grafstom, S. *J. Appl. Phys.* **2002**, *91*, 1717.
(12) Krug II, J. T.; J Sanchez, E.; Xie, X. S. *J. Chem. Phys.* **2002**, *24*, 10895.
(13) Baida, F. I.; Van Labeke, D.; Pagani, Y. *Opt. Commun.* **2003**, *225*, 241.
(14) Festy, F.; Demming, A. L.; Richards, D. *Ultramicroscopy* **2004**, *100*, 437.
(15) Demming, A. L.; Festy, F.; Richards, D. *J. Chem. Phys.* **2005**, *122*, 184716.
(16) Taflove, A.; Hagness, S. C. *Computational Electrodynamics: The Finite-Difference Time-Domain Method*, 3rd ed.; Artech House: Boston, 2005.
(17) Berenger, J.-P. *Perfectly Matched Layer (PML) for Computational Electromagnetics*; Morgan & Claypool Publishers: San Francisco, 2007.
(18) Sukharev, M.; Sung, J.; Spears, K. G.; Seideman, T. *Phys. Rev. B* **2007**, *76*, 184302.
(19) Joseph, R. M.; Hagness, S. C.; Taflove, A. *Opt. Lett.* **1991**, *16*, 1412.
(20) Hao, F.; Nordlander, P. *Chem. Phys. Lett.* **2007**, *446*, 115.
(21) (a) Rakić, A. D.; Djurišić, A. B.; Elazar, J. M.; Majewski, M. L. *Appl. Opt.* **1998**, *37*, 5271. (b) Gray, S. K.; Kupka, T. *Phys. Rev. B* **2003**, *68*, 045415.
(22) Krenn, J. R.; Schider, G.; Rechberger, W.; Lamprecht, B.; Leitner, A.; Aussenegg, F. R.; Weeber, J. C. *Appl. Phys. Lett.* **2000**, *77*, 3379.
(23) Imura, K.; Nagahara, T.; Okamoto, H. *J. Chem. Phys.* **2005**, *122*, 154701.
(24) Kreibig, U.; Vollmer, M. *Optical Properties of Metal Clusters*; Springer: New York, 1995.
(25) Wei, H.; Hao, F.; Huang, Y.; Wang, W.; Nordlander, P.; Xu, H. *Nano Lett.* **2008**, *8*, 2497.

JP900877M